Scalable Multi-View Subspace Clustering with Tensorized Anchor Guidance

Supplementary Material

7. Preliminary

Additional tensor operations and definitions are presented as follows.

Definition 3 *For a tensor $\mathcal{B} \in \mathbb{R}^{n_1 \times n_2 \times n_3}$, the block diagonal matrix and opposite operation are defined by*

$$\begin{aligned} \operatorname{bdiag}(\mathcal{B}) &= \begin{bmatrix} \mathcal{B}^1 & & \\ & \ddots & \\ & & \mathcal{B}^{n_3} \end{bmatrix}, \\ \operatorname{bdfold}(\operatorname{bdiag}(\mathcal{B})) &= \mathcal{B}. \end{aligned} \tag{19}$$

Definition 4 *For a tensor $\mathcal{B} \in \mathbb{R}^{n_1 \times n_2 \times n_3}$, its block circulant matrix is defined by*

$$\operatorname{bcirc}(\mathcal{B}) = \begin{bmatrix} \mathcal{B}^1 & \mathcal{B}^{n_3} & \cdots & \mathcal{B}^2 \\ \mathcal{B}^2 & \mathcal{B}^1 & \cdots & \mathcal{B}^3 \\ \vdots & \vdots & \ddots & \vdots \\ \mathcal{B}^{n_3} & \mathcal{B}^{n_3-1} & \cdots & \mathcal{B}^1 \end{bmatrix}. \tag{20}$$

Definition 5 *For a tensor $\mathcal{B} \in \mathbb{R}^{n_1 \times n_2 \times n_3}$, we have*

$$\begin{aligned} &\operatorname{unfold}(\mathcal{B}) = \left[\mathcal{B}^1, \mathcal{B}^2, \ldots, \mathcal{B}^{n_3}\right], \\ &\operatorname{fold}\big(\operatorname{unfold}(\mathcal{B})\big) = \mathcal{B}. \end{aligned} \tag{21}$$

Definition 6 (t-product) *Let $\mathcal{B} \in \mathbb{R}^{n_1 \times n_2 \times n_3}$ and $\mathcal{C} \in \mathbb{R}^{n_2 \times n_4 \times n_3}$, the tensor product (t-product) between them is defined by*

$$\mathcal{D} = \mathcal{B} * \mathcal{C} := \operatorname{fold}\big(\operatorname{bcirc}(\mathcal{B}) \cdot \operatorname{unfold}(\mathcal{C})\big), \tag{22}$$

where $\mathcal{D} \in \mathbb{R}^{n_1 \times n_4 \times n_3}$, and the t-product in (22) can be evaluated efficiently in the Fourier domain. Specifically, the frontal slices of $\widehat{\mathcal{B}}$ and $\widehat{\mathcal{C}}$ are multiplied slice by slice to obtain $\widehat{\mathcal{D}}$, and then the inverse transform $\mathcal{D} = \operatorname{ifft}(\widehat{\mathcal{D}}, [\,], 3)$ is applied.

Definition 7 (orthogonal tensor) *A tensor $\mathcal{B} \in \mathbb{R}^{n_1 \times n_2 \times n_3}$ is termed orthogonal if it satisfies*

$$\mathcal{B}^\top * \mathcal{B} = \mathcal{B} * \mathcal{B}^\top = \mathcal{I}. \tag{23}$$

Here, $*$ denotes the t-product, while $\mathcal{B}^\top$ and $\mathcal{I}$ represent the tensor transpose and identity tensor, respectively.

Definition 8 (f-diagonal tensor) *A tensor is termed f-diagonal if each of its frontal slices is a diagonal matrix.*

Algorithm 2 GST algorithm

Input: $\sigma_i(\mathbf{Q})$, β, p, L.
Output: δ_i^*.

```
Update τ_p(β) by using Eq. (25);
if σ_i(Q) > τ_p(β) then
    δ_i^(0) = σ_i(Q);
    for l = 0, 1, ..., L do
        δ_i^(l+1) = σ_i(Q) − βp(δ_i^(l))^(p−1);
    end for
    δ_i^* = δ_i^(L+1);
else
    δ_i^* = 0;
end if
```

Definition 9 (tensor nuclear norm) *For a tensor $\mathcal{B} \in \mathbb{R}^{n_1 \times n_2 \times n_3}$ and $h = \min(n_1, n_2)$, the tensor nuclear norm of $\mathcal{B}$ is defined by*

$$\|\mathcal{B}\|_{\circledast} = \sum_{i=1}^{n_3} \sum_{j=1}^{h} \left|\widehat{\mathcal{S}}_{\mathcal{B}}^i(j,j)\right|, \tag{24}$$

where $\widehat{\mathcal{S}}_{\mathcal{B}}^i$ can be obtained from Eq. (1).

8. Optimization

The detailed solution process for problem (13) in Section 4.3 is presented below.

According to Theorem 1, the matrix form problem (12) can be reformulated as the ℓ_p minimization problem (13). However, directly solving (13) remains computationally challenging due to the exponent p. To address this, we employ the Generalized Soft-Thresholding (GST) algorithm. The specific solution procedure is established in the following lemma.

Lemma 1. *For fixed parameters p and β, we define the critical threshold $\tau_p(\beta)$ as*

$$\tau_p(\beta) = \big(2\beta(1-p)\big)^{\frac{1}{2-p}} + \beta p\big(2\beta(1-p)\big)^{\frac{p-1}{2-p}}. \tag{25}$$

Consequently, the global optimal solution to the ℓ_p-minimization problem (13) is determined by

$$\delta_i^* = \begin{cases} 0, & \text{if } \sigma_i(\mathbf{Q}) \le \tau_p(\beta), \\ \operatorname{sign}\left(\sigma_i(\mathbf{Q})\right) S_p\left(\sigma_i(\mathbf{Q}), \beta\right), & \text{if } \sigma_i(\mathbf{Q}) > \tau_p(\beta), \end{cases} \tag{26}$$

Table 5. Fscore comparison of the proposed SMVS-TAG method and ten large-scale MVC methods on seven multi-view datasets. The best and second-best results are represented by bold and underlined values, respectively. 'OT' indicates the "out-of-time error", 'OM' means the "out-of-memory error".

Datasets	LMVSC (AAAI'20)	3AMVC (MM'24)	SMVAGC (TIP'24)	AEVC (CVPR'24)	MVSC-HFD (IF'24)	MCHBG (IF'25)	LMTC (CVPR'25)	Orth-NTF (NeurIPS'23)	TBGL (TPAMI'22)	TC-MVSC (TPAMI'24)	Proposed
					Fscore(%)						
Dermatology	77.62	57.99	68.95	<u>90.62</u>	81.98	64.62	85.53	35.57	88.94	86.98	**96.25**
Scene15	25.16	23.13	27.79	29.91	26.61	21.02	28.26	<u>33.87</u>	13.34	17.51	**45.92**
COIL100	57.93	57.83	61.84	70.05	37.24	3.28	<u>83.83</u>	28.54	69.89	11.46	**89.22**
Hdigit	42.66	73.87	56.82	<u>80.86</u>	61.00	33.14	72.63	69.20	OM	OT	**85.64**
VGGFace	2.31	2.59	4.10	2.50	2.93	OM	<u>4.24</u>	OM	OM	OM	**4.41**
AwA	3.83	3.98	3.84	4.15	OM	OM	<u>5.16</u>	OM	OM	OM	**5.33**
YoutubeFace	7.74	6.12	6.14	9.61	OM	OM	<u>11.46</u>	OM	OM	OM	**14.10**

Table 6. Ablation study of tensor anchor (TA) strategy on all datasets.

Datasets	Strategies	ACC	NMI	Purity	Fscore
Dermatology	w/o. TA	92.46	85.54	92.46	87.29
	Proposed	**97.49**	**94.02**	**97.49**	**96.25**
Scene15	w/o. TA	50.95	47.29	54.54	36.09
	Proposed	**61.00**	**55.83**	**63.39**	**45.92**
COIL100	w/o. TA	81.74	92.22	84.44	69.84
	Proposed	**90.60**	**96.49**	**92.25**	**89.22**
Hdigit	w/o. TA	86.20	77.30	86.20	76.82
	Proposed	**92.52**	**83.96**	**92.52**	**85.64**
VGGFace	w/o. TA	7.04	12.70	7.92	2.67
	Proposed	**10.67**	**18.64**	**11.70**	**4.41**
AwA	w/o. TA	10.50	12.78	12.75	5.29
	Proposed	**11.45**	**13.10**	**13.65**	**5.33**
YoutubeFace	w/o. TA	26.31	26.20	34.18	14.03
	Proposed	**36.62**	**31.48**	**43.06**	**14.10**

where the term $S_p\left(\sigma_i(\mathbf{Q}),\beta\right)$ *satisfies the implicit equation*

$$S_p\left(\sigma_i(\mathbf{Q}),\beta\right)-\sigma_i(\mathbf{Q})+\beta p\left(S_p\left(\sigma_i(\mathbf{Q}),\beta\right)\right)^{p-1}=0. \quad (27)$$

The implementation details for solving problem (13) are summarized in Algorithm 2.

9. Experimental results

9.1. Compared methods

We evaluate the proposed algorithm against ten state-of-the-art methods with linear time complexity, including

- **Large-scale Multi-view Subspace Clustering in Linear Time (LMVSC) [13]**: LMVSC leverages anchor-based graph learning to efficiently perform multi-view subspace clustering with linear complexity on large-scale data.
- **Automatic and Aligned Anchor Learning Strategy for Multi-View Clustering (3AMVC) [20]**: A hierarchical bipartite neighbor clustering algorithm is proposed to automatically identify high-quality anchors without predefining their number, and a multi-view anchor graph fusion framework is designed to align and integrate anchor graphs across views with inconsistent anchor numbers.
- **Scalable and Structural Multi-View Graph Clustering With Adaptive Anchor Fusion (SMVAGC) [35]**: This method proposes a scalable framework that jointly optimizes flexible anchor learning and graph fusion by a novel structural alignment regularization to fuse multiple anchor graphs with different magnitudes.
- **Learn from View Correlation: An Anchor Enhancement Strategy for Multi-view Clustering (AEVC) [17]**: This method proposes a plug-and-play anchor enhancement strategy that constructs a view graph to capture inter-view correlations, utilizing information from neighboring views to refine anchor distributions.
- **Anchor-based Multi-view Subspace Clustering with Hierarchical Feature Descent (MVSC-HFD) [22]**: The method projects multi-view data into a shared low-dimensional space through hierarchical projection matrices and jointly learns a common subspace to integrate the clustering of different views into a unified framework.
- **Multi-view clustering via high-order bipartite graph fusion (MCHBG) [50]**: High-order bipartite graphs are constructed to capture rich structural information with linear complexity, and a selective fusion mechanism with Laplacian rank constraints is employed to mitigate the impact of low-quality views.
- **Tensorized Bipartite Graph Learning for Multi-View Clustering (TBGL) [41]**: A tensorized bipartite graph framework is constructed using variance-based decorrelated anchors and Schatten p-norm regularization to jointly exploit inter-view and intra-view correlations.
- **Orthogonal Non-negative Tensor Factorization based Multi-view Clustering (Orth-NTF) [14]**: This method performs orthogonal non-negative tensor factorization on an anchor graph tensor and incorporates Schatten p-norm regularization to capture high-order complementary information across views.
- **Tensorized and Compressed Multi-View Subspace**

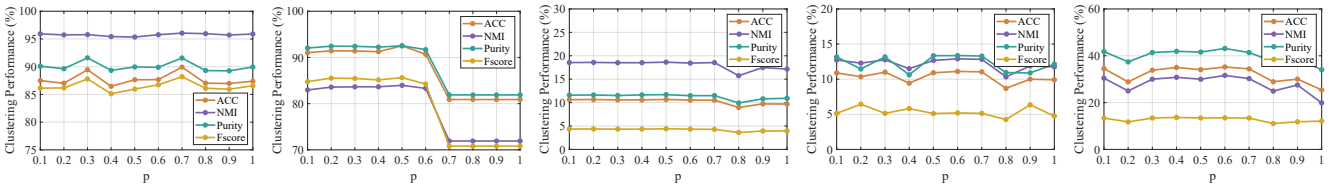

(a) COIL100 (b) Hdigit (c) VGGFace (d) AwA (e) YoutubeFace

Figure 7. Parameter sensitivity analysis of p on other five datasets.

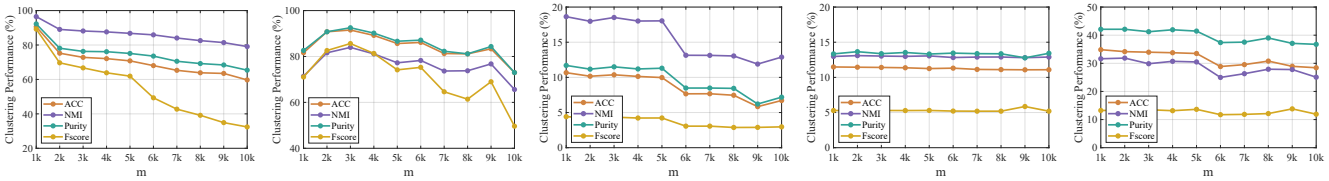

(a) COIL100 (b) Hdigit (c) VGGFace (d) AwA (e) YoutubeFace

Figure 8. Parameter sensitivity analysis of m on other five datasets.

Clustering via Structured Constraint (TC-MVSC) [1]: This method introduces a compressed subspace learning approach using low-rank tensor constraints to align dictionary-based representations, enabling direct clustering via a structured bipartite graph.

- **Large-scale Multi-view Tensor Clustering with Implicit Linear Kernels (LMTC) [16]**: This method addresses the inadvertent label leakage in tensor rotation by proposing a large-scale framework that utilizes implicit linear kernels to capture pair-wise similarities with linear complexity.

9.2. Experimental results on Fscore

The comprehensive Fscore results on seven benchmark datasets are presented in Table 5. Consistent with the metrics reported in the main text, SMVS-TAG demonstrates dominant performance across all datasets, achieving the highest Fscores. Notably, SMVS-TAG exhibits remarkable improvements on more scenarios, surpassing the second-best methods by approximately 35.58% on Scene15 and 23.04% on the large-scale YoutubeFace dataset. Furthermore, while several state-of-the-art competitors (TBGL, Orth-NTF, and MVSC-HFD) fail to yield results on heavy-load datasets like Hdigit, AwA, and VGGFace due to memory or time constraints, SMVS-TAG maintains stability and delivers the best Fscores. This further validates that the proposed tensorized anchor guidance strategy effectively enhances clustering robustness and scalability.

9.3. Other experimental results of Sec. 5.4

Table 6 presents the complete ablation study results across all seven benchmark datasets. Consistent with the findings in the main text, the introduction of the Tensor Anchor (TA) regularization yields uniform performance improvements on all datasets and evaluation metrics. Notably, this advantage is particularly pronounced on large-scale and complex datasets such as VGGFace and YoutubeFace. For instance, on YoutubeFace, the TA strategy boosts the ACC from 26.31% to 36.62%, and on VGGFace, it improves the ACC by approximately 51.56%. These results indicate that while learning view-specific anchors in a latent space provides a solid baseline, it is the tensor Schatten p-norm constraint that effectively filters out noise and enforces strict cross-view consistency. This capability is indispensable for handling the high dimensionality and heterogeneity inherent in large-scale multi-view data, ensuring that the learned anchors are not only representative but also structurally aligned.

9.4. Other experimental results of Sec. 5.5

Additional sensitivity analysis of p. Fig. 7 illustrates the impact of the parameter p on the clustering performance across the remaining five datasets: COIL100, Hdigit, VGGFace, AwA, and YoutubeFace. Consistent with the observations in the main text, the proposed SMVS-TAG demonstrates robust performance when p is selected within the range of $[0.1, 0.6]$. However, a discernible performance degradation occurs as p increases towards 1. This trend is particularly pronounced on the Hdigit dataset, where the clustering metrics drop precipitously when p exceeds 0.6, and on YoutubeFace, where the performance peaks at $p = 0.6$ before declining. These results further empirically validate that the non-convex tensor Schatten p-norm ($0 < p < 1$) offers a tighter approximation to the tensor rank than the convex nuclear norm ($p = 1$), thereby more effectively capturing the intrinsic low-rank structures in diverse multi-view datasets.

Additional sensitivity analysis of m. Fig. 8 depicts the

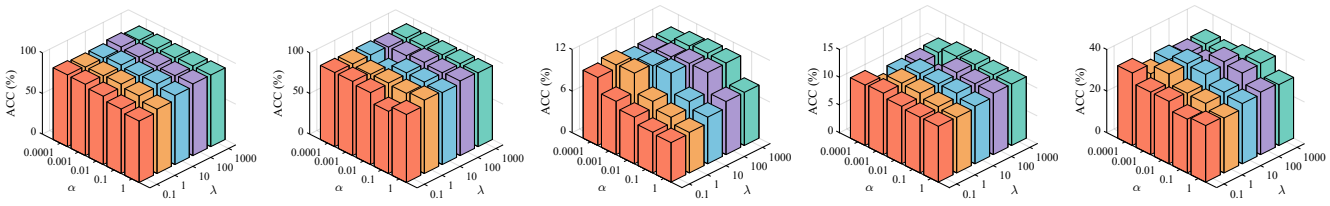

(a) COIL100 (b) Hdigit (c) VGGFace (d) AwA (e) YoutubeFace

Figure 9. Parameter sensitivity analysis of α and λ on other five datasets.

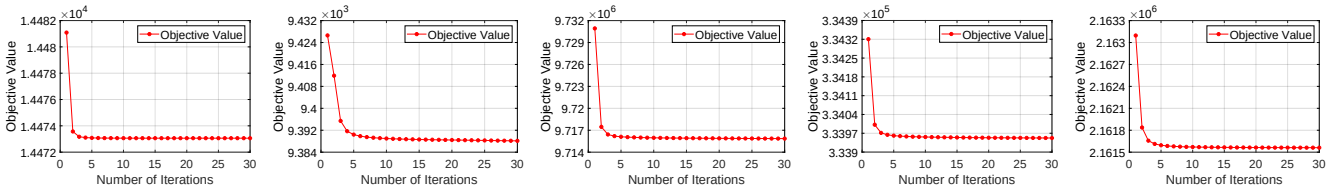

(a) COIL100 (b) Hdigit (c) VGGFace (d) AwA (e) YoutubeFace

Figure 10. The convergence analysis of our proposed method on other five datasets.

clustering performance with respect to the anchor number m (ranging from $1k$ to $10k$) on other datasets. As illustrated, simply increasing the number of anchors does not guarantee improved performance. For instance, on COIL100, the accuracy exhibits a monotonic decrease as m increases, achieving its peak at $m = 1k$. Similarly, on Hdigit, VGGFace, and YoutubeFace, the performance remains relatively stable or peaks within the range of $[2k, 5k]$, but suffers from a noticeable degradation when m exceeds $5k$. The AwA dataset shows insensitivity to variations in m, maintaining stable performance across the entire range. These observations suggest that an excessive number of anchors may introduce redundant or noisy information, which disrupts the low-rank structure of the anchor tensor. Therefore, restricting m to be no greater than $5k$ is a robust strategy that balances clustering accuracy with computational efficiency across diverse datasets.

Additional sensitivity analysis of α and λ. We further investigate the joint influence of the trade-off parameters α and λ on the remaining five datasets, as illustrated in Fig. 9. The results show that SMVS-TAG maintains robust clustering performance across a wide range of parameter combinations. Specifically, on COIL100 and Hdigit, the performance surface is remarkably flat, indicating that the method is largely insensitive to variations in α and λ on these datasets. For the large-scale and more complex datasets such as VGGFace, AwA, and YoutubeFace, a consistent pattern emerges where optimal performance is generally achieved with a smaller α combined with a larger λ. This observation aligns with the findings in the main text, suggesting that suppressing the view-specific reconstruction loss while emphasizing the consensus graph regularization aids in filtering out noise and learning a more discriminative consensus graph in complex scenarios.

Table 7. A brief summary of other multi-view datasets.

Datasets	n	k	v	$d_i (i = 1, \ldots, v)$
Yale	165	15	3	4096/3304/6750
3-sources	169	6	3	3560/3631/3068
MSRCV1	210	7	6	1302/48/512/100/256/210
ORL_mtv	400	40	3	4096/3304/6750
ForestTypes	523	4	3	9/9/9
BBCSport	544	5	2	3183/3203
MFeat_2Views	2000	10	2	76/240
HandWritten	2000	10	6	240/76/216/47/64/6
Uci_digit	2000	10	3	64/76/216
Caltech101-20	2386	20	6	48/40/254/1984/512/928
CCV	6773	20	3	20/20/20
MNIST	10000	10	3	30/9/30
Fashion	10000	10	3	784/784/784
SUNRGBD	10335	45	2	4096/4096
NUS	30000	31	5	65/226/145/74/129

9.5. Other experimental results of Sec. 5.6

We additionally evaluate the convergence behavior of SMVS-TAG on the remaining five datasets, as illustrated in Fig. 10. Consistent with the findings reported in the main text, the objective function values on all these datasets exhibit a sharp, monotonic decline during the initial iterations and rapidly converge to a stable local optimum. Notably, even on large-scale datasets such as AwA and YoutubeFace, the algorithm achieves steady-state performance within approximately 15 iterations. This empirical evidence further corroborates the high computational efficiency and robust convergence properties of our proposed optimization algorithm, validating its suitability for large-scale multi-view clustering tasks.

10. Results on other datasets

To further evaluate the generalizability and robustness of SMVS-TAG across diverse data modalities and scales, we conduct extensive experiments on fifteen additional benchmark datasets. As summarized in Table 7, these datasets span a wide spectrum of modalities, including face recognition (Yale, ORL_mtv), text categorization (3-sources, BBCSport), handwritten digit recognition (MNIST, HandWritten), and large-scale object classification (SUNRGBD, NUS). Notably, the datasets exhibit significant variations in sample size , number of views, and feature dimensionality. The comprehensive clustering results, including ACC, NMI, Purity, and Fscore, are summarized in Table 8. From these quantitative comparisons, we derive the following insights

- **Superior generalization capability.** SMVS-TAG consistently dominates the leaderboard, achieving the best performance on the vast majority of datasets ranging from small-scale text data (3-sources) to large-scale image collections (MNIST, Fashion). For instance, on the 3-sources dataset, our method improves ACC by over 20% compared to the second-best method SMVAGC. This indicates that our tensorized anchor guidance strategy effectively captures the underlying multi-view structures regardless of the data size or category.
- **Robustness against memory bottlenecks.** A critical observation from Table 8 is the stability of SMVS-TAG on large-scale and high-dimensional datasets such as NUS, SUNRGBD, and MNIST. While conventional tensor-based methods (TBGL, Orth-NTF) and some bipartite graph approaches (MCHBG) frequently fail due to "out-of-memory" (OM) errors, our method successfully yields high-quality clustering results. This reinforces the advantage of applying tensor constraints on the compact anchor space rather than the full sample space, ensuring scalability without compromising performance.
- **Advantage over recent competitors.** Even when compared with the most recent state-of-the-art methods (AEVC, LMTC, 3AMVC), SMVS-TAG maintains a distinct competitive edge. Unlike AEVC and 3AMVC, which focus on graph fusion or anchor selection independently, our approach jointly optimizes view-specific anchors within a unified tensor framework. This holistic optimization allows SMVS-TAG to better exploit complementary information, resulting in significant margins on more datasets like MFeat_2Views and SUNRGBD, where we surpass the second-best methods by approximately 4.34% and 19.27% in ACC, respectively.

Table 8. Clustering performance comparison of the proposed SMVS-TAG method and ten large-scale MVC methods on other multi-view datasets. The best and second-best results are represented by bold and underlined values , respectively. 'OM' means the "out-of-memory error".

Datasets	LMVSC (AAAI'20)	3AMVC (MM'24)	SMVAGC (TIP'24)	AEVC (CVPR'24)	MVSC-HFD (IF'24)	MCHBG (IF'25)	LMTC (CVPR'25)	Orth-NTF (NeurIPS'23)	TBGL (TPAMI'22)	TC-MVSC (TPAMI'24)	Proposed
ACC(%)											
Yale	54.55	59.04	64.10	65.99	50.30	48.48	71.52	64.24	67.88	60.61	**78.79**
3-sources	54.44	49.23	65.31	59.85	44.38	64.50	57.99	35.50	37.87	34.91	**81.07**
MSRCV1	80.48	84.69	74.25	82.98	89.52	66.67	91.43	80.95	80.95	85.71	**92.38**
ORL_mtv	63.00	64.69	71.09	65.66	49.25	58.75	81.75	73.25	72.00	63.25	**83.00**
ForestTypes	80.69	71.86	74.10	82.88	71.70	56.60	72.47	57.17	71.13	48.18	**85.66**
BBCSport	51.65	53.82	71.56	69.86	52.39	54.78	70.59	68.38	46.14	35.48	**81.07**
MFeat_2Views	84.50	83.77	71.69	83.68	81.05	76.85	88.65	79.45	75.00	70.35	**92.50**
HandWritten	85.40	77.68	79.29	88.78	63.40	95.00	92.95	92.20	86.30	76.15	**95.85**
Uci_digit	84.95	87.56	85.53	89.22	81.35	80.40	93.35	89.15	84.60	75.65	**94.45**
Caltech101-20	20.16	41.81	38.19	42.93	52.98	38.98	48.32	51.76	62.11	46.90	**65.67**
CCV	20.73	17.47	23.44	24.07	20.48	12.31	22.94	15.40	11.34	15.92	**25.84**
MNIST	44.74	56.60	82.97	63.35	82.46	49.81	65.21	64.48	OM	55.36	**86.19**
Fashion	54.62	75.45	78.67	77.92	70.18	32.69	76.33	30.15	OM	57.58	**85.34**
SUNRGBD	16.73	15.94	18.96	16.40	22.37	14.52	20.38	15.30	OM	10.94	**26.68**
NUS	14.44	12.22	11.68	14.52	18.05	OM	12.37	OM	OM	OM	**18.61**
NMI(%)											
Yale	61.05	64.63	69.75	69.35	52.16	54.64	69.97	73.34	69.10	62.42	**77.72**
3-sources	43.85	38.69	57.26	47.95	33.71	45.41	56.68	19.91	7.37	6.80	**69.55**
MSRCV1	76.78	76.63	66.59	74.31	84.20	59.37	83.83	75.21	80.36	81.34	**85.01**
ORL_mtv	82.45	82.75	86.85	82.76	70.33	69.05	90.49	84.41	80.11	75.08	**91.38**
ForestTypes	55.83	47.71	47.79	59.50	42.19	28.40	41.16	28.20	43.62	33.48	**63.02**
BBCSport	38.16	33.80	57.49	44.79	20.73	43.79	**62.79**	60.12	13.66	1.02	60.89
MFeat_2Views	81.19	79.87	68.52	74.70	72.62	75.06	79.65	83.33	82.67	67.88	**85.64**
HandWritten	80.81	73.91	68.74	81.17	66.03	90.20	85.53	89.32	87.34	74.03	**91.48**
Uci_digit	77.97	82.43	76.67	80.23	80.36	80.02	86.38	85.16	87.44	74.32	**88.59**
Caltech101-20	41.84	47.21	44.44	56.04	52.14	33.57	59.16	58.74	49.95	57.71	**64.19**
CCV	16.81	12.93	19.21	18.10	15.28	3.04	19.63	9.02	1.66	11.35	**20.62**
MNIST	44.91	50.62	72.14	57.91	70.47	54.59	63.30	70.38	OM	54.27	**73.41**
Fashion	52.24	74.44	75.38	70.07	77.46	28.42	74.80	17.41	OM	59.99	**79.92**
SUNRGBD	22.99	15.86	20.78	20.72	22.37	14.14	24.49	22.07	OM	1.03	**24.69**
NUS	11.09	11.01	10.40	12.56	12.32	OM	10.08	OM	OM	OM	**13.37**
Purity(%)											
Yale	66.06	60.58	65.54	66.50	50.30	49.09	71.52	64.85	67.88	60.61	**78.79**
3-sources	**86.98**	60.06	73.49	67.56	57.40	68.05	78.70	50.89	38.46	36.09	82.25
MSRCV1	85.24	84.90	76.64	82.99	89.52	66.67	91.43	80.95	81.43	85.71	**92.38**
ORL_mtv	71.75	68.73	74.83	69.91	50.75	65.25	84.00	75.00	76.00	70.25	**84.75**
ForestTypes	80.69	74.37	74.51	82.88	71.70	56.98	72.47	61.19	71.13	58.89	**85.66**
BBCSport	57.90	59.14	74.97	69.86	52.76	61.95	81.07	80.15	46.14	36.03	**81.07**
MFeat_2Views	84.50	84.91	74.67	83.94	81.05	76.85	88.65	83.05	77.65	72.25	**92.50**
HandWritten	85.40	78.35	79.77	89.26	66.65	95.00	92.95	92.20	86.30	79.60	**95.85**
Uci_digit	84.95	88.31	85.97	89.33	82.00	82.85	93.35	89.15	87.10	77.75	**94.45**
Caltech101-20	22.89	64.70	65.79	72.88	67.85	52.81	**81.10**	72.21	71.37	71.00	75.90
CCV	23.37	21.81	26.46	26.30	23.79	12.83	25.51	18.80	11.75	18.20	**29.40**
MNIST	55.49	58.38	83.89	66.50	82.46	58.66	70.32	66.74	OM	61.07	**86.19**
Fashion	60.41	78.14	80.71	78.09	70.97	35.51	77.63	30.90	OM	57.58	**85.34**
SUNRGBD	17.73	27.06	32.90	33.47	30.94	23.95	**39.20**	31.31	OM	11.45	34.18
NUS	16.93	22.72	21.30	**24.21**	23.31	OM	21.65	OM	OM	OM	23.85
Fscore(%)											
Yale	38.73	42.93	51.59	52.25	31.64	33.58	54.99	49.82	45.67	41.47	**64.65**
3-sources	48.42	40.17	61.59	49.90	37.93	62.11	56.82	29.83	38.59	38.05	**77.23**
MSRCV1	69.63	75.25	64.24	72.04	82.74	54.83	83.69	71.20	76.48	75.80	**85.17**
ORL_mtv	53.54	50.86	63.29	55.50	33.14	20.80	74.91	60.75	34.02	26.71	**75.29**
ForestTypes	67.55	59.81	59.47	70.71	55.78	53.58	56.15	43.41	55.54	49.80	**74.35**
BBCSport	39.37	40.69	59.77	51.16	39.31	52.73	66.71	61.36	41.02	38.26	**71.19**
MFeat_2Views	77.44	75.95	63.07	73.27	68.32	68.50	79.34	76.40	77.12	50.40	**85.72**
HandWritten	77.57	65.34	67.45	81.12	55.81	89.97	86.51	86.98	83.60	69.32	**91.80**
Uci_digit	73.13	79.72	75.77	80.35	76.22	73.49	87.24	80.84	83.58	60.16	**89.29**
Caltech101-20	16.51	35.87	33.68	34.89	54.17	23.63	41.36	45.40	45.85	31.32	**65.41**
CCV	11.60	10.42	13.62	13.08	12.15	10.95	13.62	8.59	10.84	10.35	**14.51**
MNIST	35.06	38.64	73.43	53.76	71.58	41.23	58.84	60.87	OM	43.04	**75.42**
Fashion	43.09	68.13	71.66	67.90	68.79	24.32	68.85	19.55	OM	45.73	**77.67**
SUNRGBD	10.39	9.66	11.33	9.89	14.65	10.58	13.45	9.03	OM	12.15	**16.73**
NUS	9.11	7.58	7.29	8.63	12.07	OM	7.82	OM	OM	OM	**12.34**